Effects of calcium nitride and calcium carbonate gasifying agents on the combustion synthesis of Ni_3Ti-TiC composites

DOUGLAS E. BURKES*
Metallurgical and Materials Engineering Department, Colorado School of Mines, Golden, CO 80401, USA; Center for Commercial Applications of Combustion in Space, Colorado School of Mines, Golden, CO 80401, USA
E-mail: dburkes@mines.edu

HU CHUN YI
Guigne International Ltd., St. John's, NL A1L, 1C1, Canada

GUGLIELMO GOTTOLI, JOHN J. MOORE
Metallurgical and Materials Engineering Department, Colorado School of Mines, Golden, CO 80401, USA; Center for Commercial Applications of Combustion in Space, Colorado School of Mines, Golden, CO 80401, USA

Published online: 17 February 2006

The synthesis of nickel-titanium (NiTi) intermetallic composites is of considerable interest due to the ability to create a porous material with high strength and improved wear resistance. The effects of adding a carbon reactant to modify the reaction products and exothermicity have been studied using two reaction stoichiometries involving elemental nickel, titanium and carbon (graphite). The present study examines the synthesis of porous Ni_3Ti intermetallic composites in the presence of calcium nitride or calcium carbonate gasifying agent. Both gasifying agents show significant effects on the ignition characteristics of the reaction, burning velocities and TiC particle sizes present in the final product, but do not affect the combustion temperatures.

1. Introduction

Combustion synthesis is an alternative technique for producing advanced ceramics, ceramic composites and intermetallic compounds [1] and is dependent upon the ability of a highly exothermic chemical reaction to become self-sustaining after a short energy pulse is applied to initiate the reaction. In general, exothermic combustion synthesis reactions become self-sustaining at adiabatic temperatures above 1800 K and a ratio of $\Delta H(298\ K)$ to $Cp(298\ K)$ above 2000 K [2].

Porous materials have shown promise as medical devices ranging from dental implants to bone and joint replacement implants. Materials for bone and joint replacement applications typically require product porosity in the range of 40 to 60% and pore sizes between 200 and 500 microns [3]. Porous materials produced using combustion synthesis have a high volume of interconnected (open) pores providing space for vascular tissue required for continued mineralized bone growth [4, 5]. Gasifying agents are added to the reactant stoichiometry to optimize and improve the porosity of the synthesized product without retarding the combustion reaction.

A number of factors contribute to the porosity, pore size and pore distribution of the synthesized product [6]. For example, initial porosity is important due to a change in volume between the initial reactants and the synthesized products for a reaction that generates liquid at the reaction front [7]. Particle sizes of the initial reactants provide volume for conversion into pores during the combustion reaction by affecting the packing density [8, 9]. Convective flow of gas through the combustion front due to steep temperature gradients play a role in pore formation within the product [10]. Finally, addition of a gasifying agent to the combustion reaction can increase the pressure within the reaction zone resulting in the formation or

*Author to whom all correspondence should be addressed.
0022-2461
DOI: 10.1007/s10853-006-4500-z

TABLE I Physical and thermodynamic properties of the reactants and products

Element/ Compound	Melting/Boiling point (°C)	Density ($kg \cdot m^{-3}$)	Particle size (μm)	Impurity (%)
Ni	1453/2730	8900	<44	<0.1
Ti	1668/3260	4540	<44	<0.002
C (graphite)	3650/——	2260	<44	<0.5
Ca_3N_2	——/1195*	2630	<44	<0.1
$CaCO_3$	——/800*	2930	<44	<0.5
NiTi	1310/——	6941	—	—
TiC	3065/——	4940	—	—
TiN	2950/——	5400	—	—

*Decomposition temperature.

suppression of pores, depending on the type of agent selected [11]. The current investigation seeks to document the last of these factors with two novel gasifying additives, calcium nitride (Ca_3N_2) and calcium carbonate ($CaCO_3$). All of the aforementioned factors have significant advantages and/or disadvantages over the combustion synthesis process. The effects of the gasifying additives on the final product porosity, bulk density and pore size are presented in a subsequent paper [12].

2. Experimental materials and methods

Two chemistries within the Ni_3Ti-TiC system were explored designated as TiC-30wt% Ni_3Ti and TiC-50 wt% Ni_3Ti. The chemistries were combined with a varying amount (z) of calcium nitride (Ca_3N_2) or calcium carbonate ($CaCO_3$) gasifying agent in an inert argon environment as specified by the reaction systems provided in Equations 1 and 2.

$$xNi + (x + y + 2z)Ti + yC + zCa_3N_2 = xNiTi + yTiC + 2zTiN + 3zCa(g) \quad (1)$$

$$xNi + (x + y)Ti + yC + zCaCO_3 = xNiTi + yTiC + zCaO + zCO_2(g) \quad (2)$$

Elemental and Ca_3N_2 powders were obtained from Cerac, Inc. (Milwaukee, WI) while the $CaCO_3$ powder was obtained from Alfa Aesar Inc. (Ward Hill, MA). Typical physical and thermal properties of the reactants and products are provided in Table I. The adiabatic temperature of the chemistries with no gasifying additive and assuming formation of equi-atomic NiTi and stoichiometric TiC is 2965°K and 2564°K for the TiC-30 wt% Ni_3Ti and TiC-50 wt% Ni_3Ti, respectively.

Reaction stoichiometries were prepared maintaining the amount of Ni_3Ti intermetallic present in the synthesized product and the amount of gas produced from the gasifying agent. The refractory phase and decomposition product varied for differing amounts and type of gasifying agent. Three amounts of gasifying agent were investigated in addition to samples reacted with no gasifying agent. Amounts of 0.012, 0.025 and 0.036 wt% Ca_3N_2 were added to the chemistries corresponding to 1 wt%, 2 wt% and 3 wt% of calcium gas evolution during the reaction, respectively. Amounts of 0.22, 0.45 and 0.66 wt% $CaCO_3$ gasifying agent were added to the chemistries corresponding to 1 wt%, 2 wt% and 3 wt% CO_2 gas evolved during the reaction, respectively. Powder and sample preparation techniques for these chemistries have been documented elsewhere [13]. The initial relative density of each sample was determined as the actual sample density divided by the theoretical density of the chemistry. Actual density was determined by dividing the mass of the sample by the sample volume. Theoretical density was determined as the summation of the individual reactant weights multiplied by the individual reactant density. Each sample had an approximate initial relative density of 30% allowing for the maximum amount of available volume to be converted into pores.

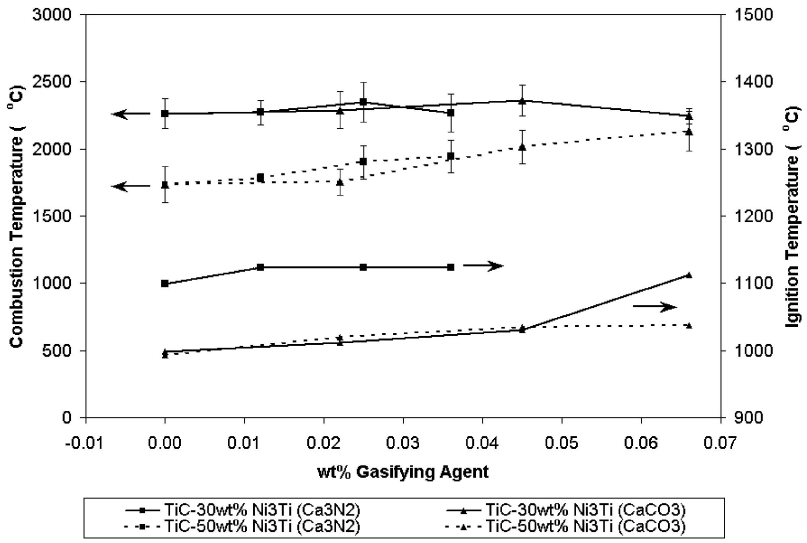

Figure 1 Combustion and ignition temperatures as a function of wt% gasifying agent.

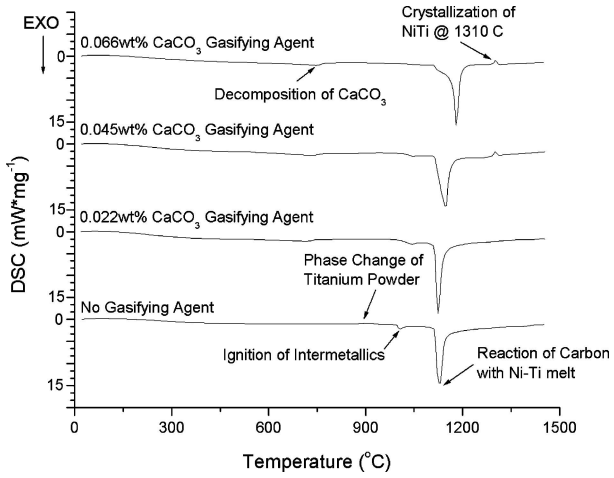

Figure 2 DSC analysis for TiC-30 wt% Ni_3Ti and increasing amounts of $CaCO_3$ gasifying agent.

Each sample was placed in a combustion chamber on a tungsten resistance heater for ignition. The chamber was vacuumed and purged with argon three times maintaining an ambient chamber pressure of 101.33 kPa. Approximately 69 Amperes were supplied to the tungsten resistance heater by a XFR 70/40 power supply (Xantrex Technologies, Burnaby, BC). Two 0.127 mm type C thermocouples were placed at the midpoint of the sample to measure combustion temperature. A PX105 0-50 psig pressure transducer was used to measure the relative pressure rise of each experiment (Omega Engineering, Stamford, CT). All data was collected at 200 Hz per channel (i.e. 0.005 sec response time) through a DAQ pad 1200 (National Instruments, Austin, TX) using a desktop computer. A Canon XL1 3CCD digital video camcorder was employed to record the combustion wave and reactant consumption of each experiment. Tracker 3 software [14] was utilized to track the combustion wave and obtain a moving average burning velocity of the reaction.

Chemical and phase analysis was conducted using a Phillips X'Pert x-ray diffraction (XRD) diffractometer

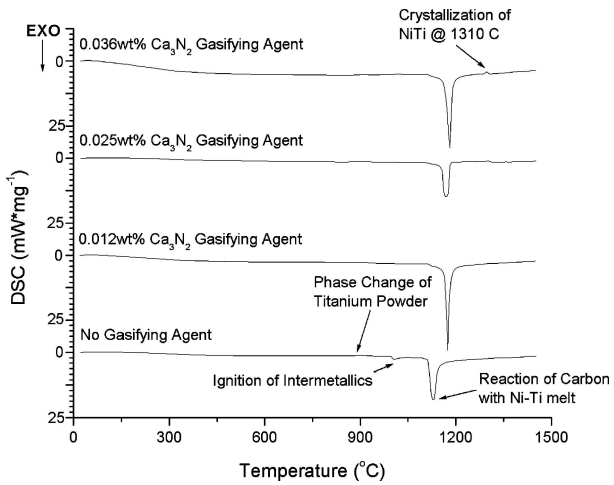

Figure 3 DSC analysis for TiC-30 wt% Ni_3Ti and increasing amounts of Ca_3N_2 gasifying agent.

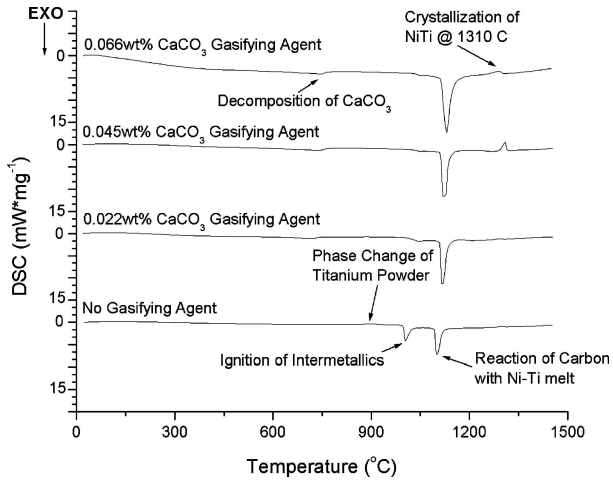

Figure 4 DSC analysis for TiC-50 wt% Ni_3Ti and increasing amounts of $CaCO_3$ gasifying agent.

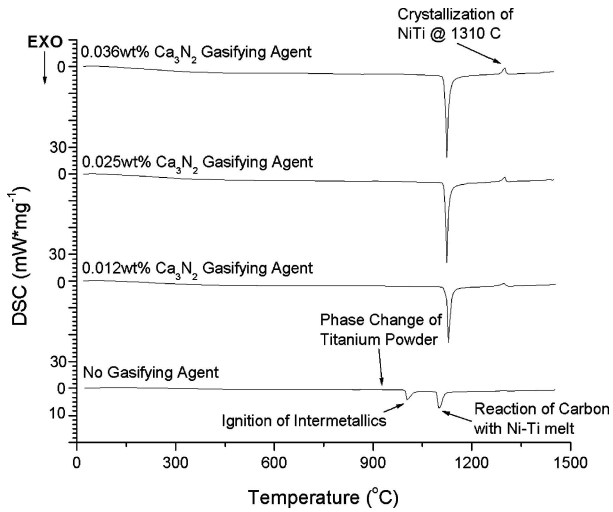

Figure 5 DSC analysis for TiC-50 wt% Ni_3Ti and increasing amounts of Ca_3N_2 gasifying agent.

with copper radiation. Scans were taken from 30° to 80° 2θ at a scan speed of $0.0150°{\cdot}sec^{-1}$ and $0.0125°{\cdot}sec^{-1}$ for the TiC-30 wt% Ni_3Ti and TiC-50 wt% Ni_3Ti, respectively. A FEI Quanta 600 environmental scanning electron microscope (ESEM) was employed to take photomicrographs. Ignition and kinetic characteristics of the chemistries were examined using a NETZSCH DSC 404 differential scanning calorimetry (DSC) analyzer. A small amount of reactant powder (~10 mg) was placed in an Al_2O_3 crucible and heated from 20°C to 1500°C at 40 $K{\cdot}min^{-1}$. Endothermic and exothermic peaks were observed and analyzed using NETZSCH software that accompanies the machine.

3. Results and discussion

3.1. Combustion synthesis analysis

Between five and ten measurements were used to determine combustion temperature, relative pressure rise and burning velocity. The data points for Figs 1, 6 and

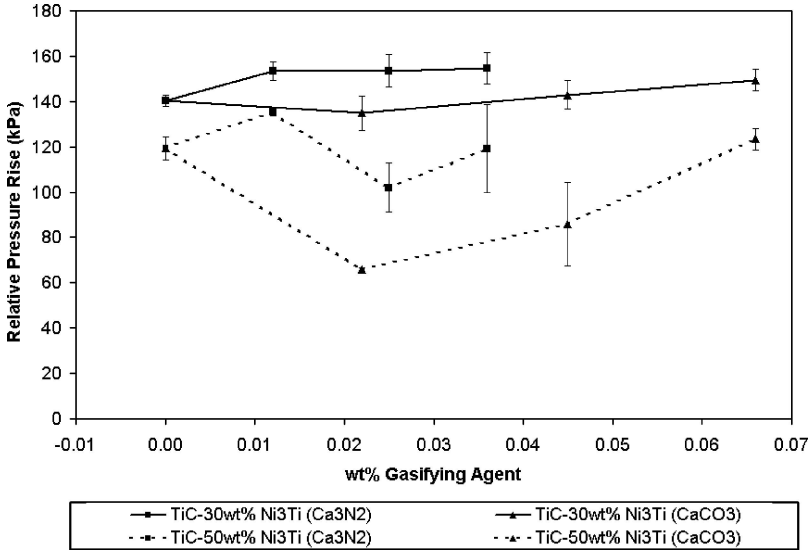

Figure 6 Relative pressure rise as a function of wt% gasifying agent.

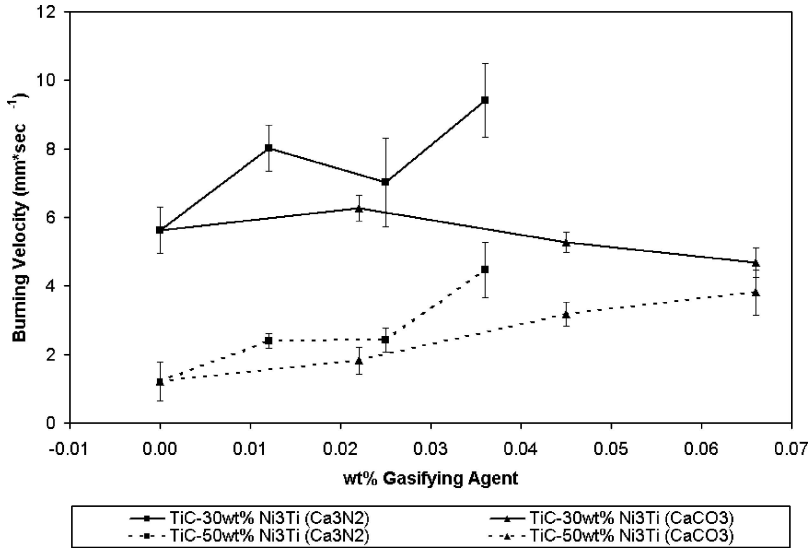

Figure 7 Burning velocity as a function of wt% gasifying agent.

7 are average values with the error bars representing the standard deviation of the sample set.

The maximum combustion temperatures recorded by the thermocouples and the ignition temperatures determined from DSC analysis are presented in Fig. 1. Data points presented for ignition temperature are onset values of the first exothermic peak observed from DSC analysis. The combustion temperature of the reactions is not affected by the addition of a $CaCO_3$ ($CaCO_3 \rightarrow CaO + CO_2$; $\Delta H(298\ K) = 178\ kJ{\cdot}mol^{-1}$) or Ca_3N_2 ($Ca_3N_2 \rightarrow 3Ca + N_2$; $\Delta H(298\ K) = 964\ kJ{\cdot}mol^{-1}$) gasifying agent. There is a slight increase in combustion temperature for the TiC-50 wt% Ni_3Ti with increasing amounts of $CaCO_3$ as a result of the thermal properties of the carbon dioxide [10] decomposition product and higher thermal diffusivity of the reactant mixture (Table I).

The reaction kinetics is affected by the addition of $CaCO_3$ gasifying agent. Ignition temperatures increased for both chemistries as the amount of $CaCO_3$ was increased in the reactant mixture. This suggests that $CaCO_3$ acts as a heat sink and results in the formation of intermetallics that are no longer the ignition mechanism. Rather decomposition of $CaCO_3$ into CO_2 followed by dissociation of CO_2 into CO, i.e. the more stable of the gases in the presence of carbon (graphite), provides a "trigger" reaction in the form of TiO_2 [10]. The highly exothermic trigger reaction locally melts the nickel and titanium reactants that spread over the graphite particles. Capillary flow of molten titanium over graphite results in a dissolution-precipitation mechanism as carbon diffuses into titanium [15]. The reaction becomes self-sustaining as a result of the latter reaction mechanism. DSC data are presented in Fig. 2 for the TiC-30 wt% Ni_3Ti and

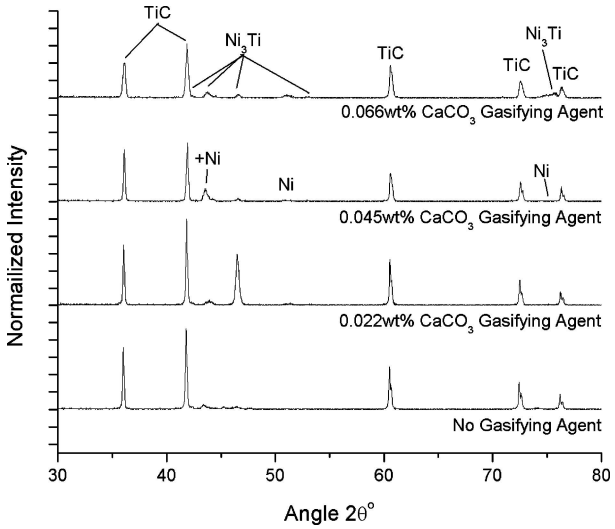

Figure 8 XRD profiles for TiC-30 wt% Ni_3Ti with $CaCO_3$ gasifying agent.

Fig. 4 for the TiC-50 wt% Ni_3Ti with the $CaCO_3$ gasifying agent. The intermetallic exotherm [10] becomes smaller and shifts to the right for increasing amounts of $CaCO_3$ gasifying agent. In addition, the second exotherm shifts to the right, representing a higher ignition temperature, and becomes more negative, representing a greater energy release from the reactant mixture. An endotherm representing the solidification temperature of NiTi (1310°C) [16] becomes evident as more $CaCO_3$ gasifying agent is added. The formation of NiTi results from the slow heating rate (40 $K \cdot min^{-1}$) employed and the slow evolution of gas during DSC analysis that disrupts molten titanium flow to the TiC nucleation sites. Thus, less titanium reacts with graphite promoting the formation of equi-atomic NiTi.

The DSC ignition analysis for the TiC-30 wt% Ni_3Ti and TiC-50 wt% Ni_3Ti with Ca_3N_2 gasifying agent are presented in Fig. 3 and Fig. 5, respectively. There is no shift in the secondary reaction exotherm, but rather only dissipation of the intermetallic exotherm as the gasifying agent is increased. Similar to results observed with the $CaCO_3$ gasifying agent, decomposition of Ca_3N_2 into calcium and nitrogen gas results in a "trigger" reaction taking on the form of TiN [10]. The highly exothermic TiN reaction (T_{ad} = 4909 K) locally melts the nickel and titanium reactants inciting a dissolution-precipitation reaction mechanism between the molten titanium and graphite particles. Opposite to the $CaCO_3$ gasifying agent, the Ca_3N_2 gasifying agent demands energy from the system to decompose, but returns energy to the system from the formation of TiN. Thus, only slight increases for ignition temperature are detected for the Ca_3N_2 gasifying agent while larger increases are observed for the $CaCO_3$.

Relative pressure rise as a function of weight percent gasifying agent is provided in Fig. 6. Relative pressure rise increased with increasing amounts of gasifying agent introduced into the TiC-30 wt% Ni_3Ti. The Ca_3N_2 additive exhibited a greater relative pressure rise than the $CaCO_3$. This is expected as decomposition of one mole of Ca_3N_2 additive yields three moles of calcium gas to only one mole of CO_2 gas produced from one mole of $CaCO_3$ additive. The volume of the combustion chamber is constant for both reactions and there is minimal variation in combustion temperature observed in Fig. 1. A similar trend is observed for the TiC-50 wt% Ni_3Ti. However, the TiC-50 wt% Ni_3Ti relative pressure rise for the $CaCO_3$ additive is closer to the Ca_3N_2 additive for additions greater than 0.045 wt% $CaCO_3$. The similarity results from increased combustion temperatures for these reactions provided in Fig. 1, thereby increasing the relative pressure rise.

Burning velocity as a function of weight percent gasifying agent is provided in Fig. 7. The burning velocity trends are expected for the TiC-30 wt% Ni_3Ti. Burning velocity increased for increasing amounts of Ca_3N_2 gasifying agent added to the chemistry. This is attributed to the evolution of nitrogen during the reaction and the addition of TiN to the reaction products subsequently increasing the reaction exothermicity. Burning velocity decreased for increasing amounts of $CaCO_3$ added to the system attributed to the energy required to decompose the gasifying agent with no additional exothermic product formation. The CaO becomes a heat sink in the reaction product while the CO_2 (CO) increases pore formation. The TiC-30 wt% Ni_3Ti has a lower thermal diffusivity than the TiC-50 wt% Ni_3Ti resulting in less heat transferred ahead of the reaction front and lower burning velocities. The TiC-50 wt% Ni_3Ti burning velocity increased for increasing amounts of both gasifying agents. The Ca_3N_2 gasifying agent increases the exothermicity

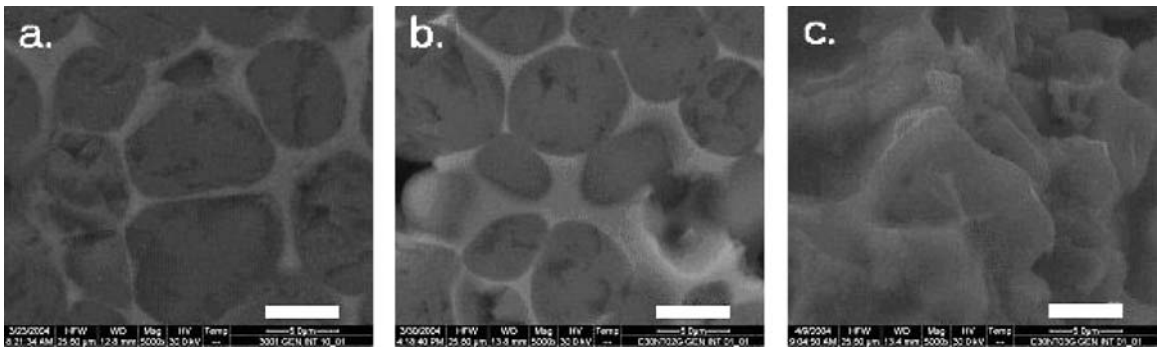

Figure 9 SEM photomicrographs of TiC-30 wt% Ni_3Ti with (a) 0.022 wt%, (b) 0.045 wt% and (c) 0.066 wt% $CaCO_3$ gasifying agent (Scale = 5.0 μm).

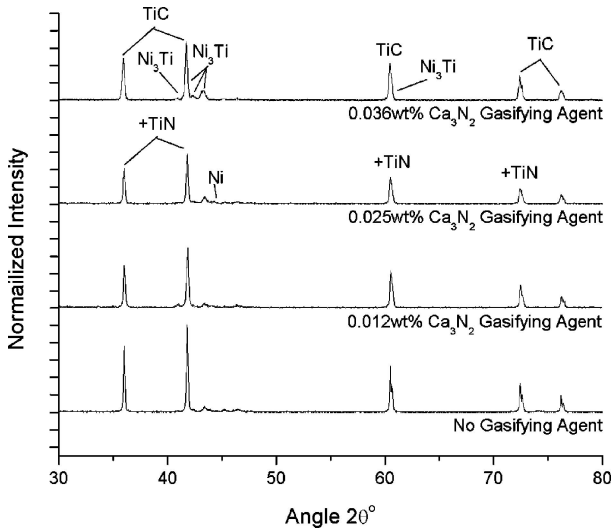

Figure 10 XRD profiles for TiC-30 wt% Ni_3Ti with Ca_3N_2 gasifying agent.

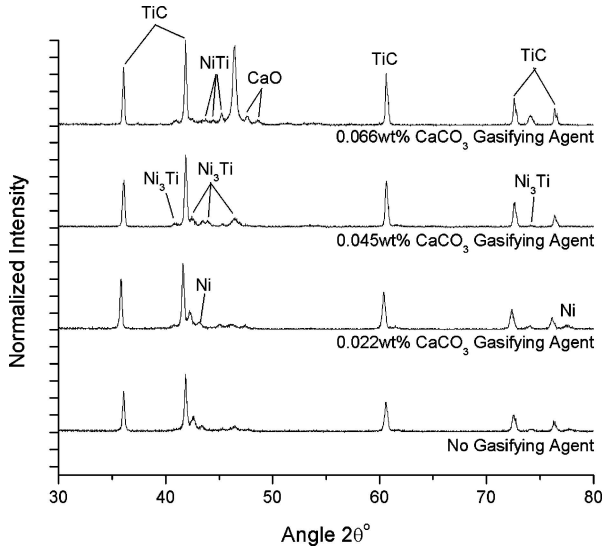

Figure 12 XRD profiles for TiC-50 wt% Ni_3Ti with $CaCO_3$ gasifying agent.

of the reaction due to the formation of TiN similar to the TiC-30 wt% Ni_3Ti. However, the $CaCO_3$ gasifying agent has an opposite trend compared to the TiC-30 wt% Ni_3Ti. The TiC-50 wt% Ni_3Ti has a higher thermal diffusivity than the TiC-30 wt% Ni_3Ti that conducts more heat ahead of the reaction front. Less carbon (graphite) is present in the TiC-50 wt% Ni_3Ti causing less dissociation of CO_2 into CO. Thus, the CO_2 contributes to heat transfer ahead of the reaction front aiding in pre-heating of the reactants and increasing the burning velocity as more CO_2 is evolved from the gasifying agent ($CaCO_3$).

4. Microstructure analysis

XRD profiles for TiC-30 wt% Ni_3Ti with $CaCO_3$ gasifying agent are provided in Fig. 8. The profiles in Fig. 8 are normalized against the 0.022 wt% $CaCO_3$ gasifying agent profile that produces the highest intensity TiC peak. The TiC peak intensities decrease and minimally shift to the left for increasing additions of $CaCO_3$ gasifying agent. Observation of the XRD figures shows that the main constituent of intermetallic produced from these reactions is Ni_3Ti. Formation of a nickel rich intermetallic is the result of substoichiometric TiC production. This effect has been observed with reactions containing no gasifying agents because substoichiometric TiC formation was not anticipated [10, 13]. The presence of excess nickel (i.e. $\geq$5 wt%) in the final product is detected for increasing amounts of $CaCO_3$ gasifying agent. The burning velocity of the reaction decreases as the amount of $CaCO_3$ gasifying agent is correspondingly increased. The cooling rate of the sample increases [17] allowing the TiC particles to grow via Ostwald ripening [18] resulting in larger TiC particles. Greater additions of $CaCO_3$ gasifying agent result in greater amounts of CO_2 gas evolved from the system. The TiC-30 wt% Ni_3Ti contains a high percentage of carbon (graphite) in the reactant mixture (i.e. 14 wt%). Previous discussion stated that CO is more stable at elevated temperatures than CO_2 in the presence of carbon. As a result, some of the carbon from the reactant mixture will combine with free oxygen from the dissociation of CO_2 into CO. More carbon is removed from the reactant mixture as the amount of $CaCO_3$ gasifying agent is increased. The increased CO_2 (CO) disrupts molten titanium flowing to the TiC nucleation sites via capillary flow. Both of these mechanisms, i.e. less titanium supply to the TiC nucleation sites and removal of carbon from the

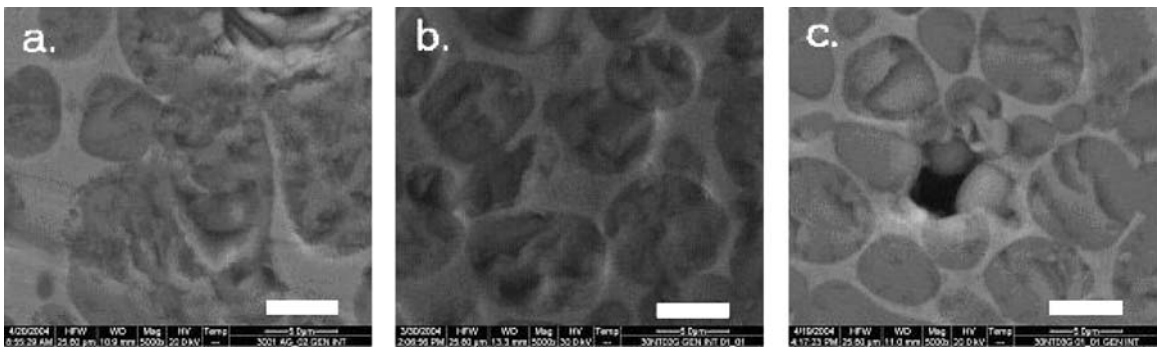

Figure 11 SEM photomicrographs of TiC-30 wt% Ni_3Ti with (a) 0.012 wt%, (b) 0.025 wt% and (c) 0.036 wt% Ca_3N_2 gasifying agent (Scale = 5.0 μm).

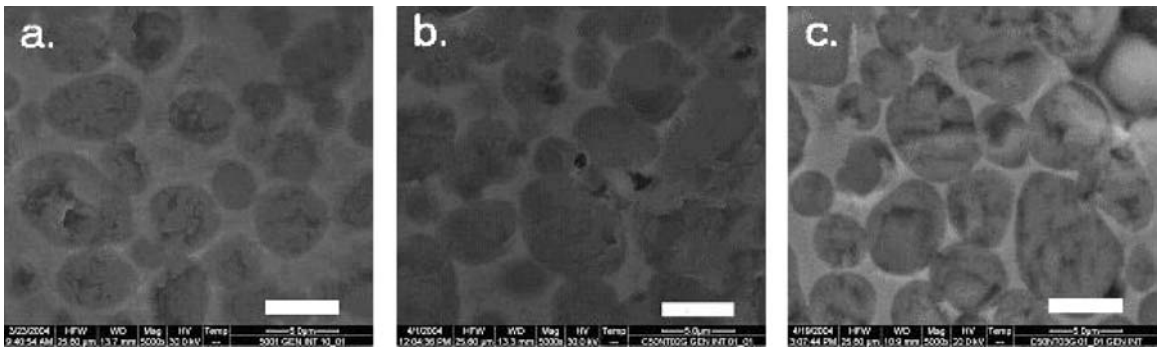

Figure 13 SEM photomicrographs of TiC-50 wt% Ni_3Ti with (a) 0.022 wt%, (b) 0.045 wt% and (c) 0.066 wt% $CaCO_3$ gasifying agent (Scale = 5.0 μm).

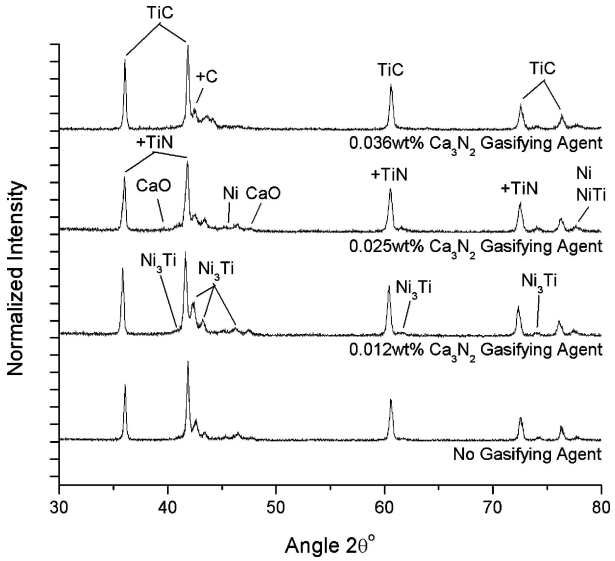

Figure 14 XRD profiles for TiC-50 wt% Ni_3Ti with Ca_3N_2 gasifying agent.

system in the form of CO, result in a more stoichiometric TiC phase, explaining the shift of the TiC peaks to the left as the amount of $CaCO_3$ added to the system is increased.

SEM photomicrographs are presented in Fig. 9 for the 0.022 wt%, 0.045 wt% and 0.066 wt% $CaCO_3$ gasifying agent with the TiC-30 wt% Ni_3Ti. These photomicrographs show the difference of TiC particle structure as the amount of gasifying agent is increased. Specifically, the TiC particles become less spherical in nature and more intermetallic phase (light gray) is observed. Less spherical TiC grains suggest a carbon diffusion mechanism rather than a carbon dissolution-precipitation mechanism that results in spherical TiC particles [19, 20]. This mechanism was also suggested from analysis of the XRD profiles provided earlier.

XRD profiles for TiC-30 wt% Ni_3Ti with Ca_3N_2 gasifying agent are provided in Fig. 10. The profiles in Fig. 10 are normalized against the profile with no gasifying agent that produces the highest intensity TiC peak. TiC peak intensity decreased with increasing amounts of Ca_3N_2 gasifying agent but there was no observable shift in the location of the TiC peaks. TiN peaks overlap with TiC peaks, but trace amounts of TiN in the microstructure are present based on kinetic analysis and discussion provided earlier. Trace amounts of nickel are also observed in the XRD profiles. The amount of Ni_3Ti (as a result of substoichiometric TiC formation) increased with increasing Ca_3N_2 gasifying agent.

SEM photomicrographs of the 0.012 wt%, 0.025 wt%, and 0.036 wt% Ca_3N_2 gasifying agent added to the TiC-30 wt% Ni_3Ti chemistry are presented in Fig. 11. These photomicrographs do not reveal differences on the TiC structure when compared to the $CaCO_3$ additive. This results from calcium gas having less of an impact on the molten titanium. Decomposing calcium and nitrogen gas does not remove any carbon from the reactant mixture. The TiC particle size decreased while the number of particles increased as the amount of Ca_3N_2 gasifying agent was increased. Burning velocity increased with increasing amounts of Ca_3N_2 effectively decreasing the cooling time of the sample. The decreased cooling time results in less Ostwald ripening and smaller TiC particles that are greater in number.

XRD profiles for TiC-50 wt% Ni_3Ti with $CaCO_3$ gasifying agent are provided in Fig. 12. Profiles in Fig. 12 are normalized against the 0.066 wt% $CaCO_3$ gasifying agent profile that produces the highest intensity TiC peak. The intensity of the TiC and Ni_3Ti peaks increased with increasing amounts of $CaCO_3$ gasifying agent. No shift in the TiC peaks was observed as a result of decreased carbon content (i.e. 10 wt%) with the TiC-50 wt% Ni_3Ti. The decrease in reactant carbon and the lower combustion temperatures permit the CO_2 to remain stable rather than dissociating into CO. There are trace amounts of CaO decomposition product and nickel in the XRD patterns.

SEM photomicrographs of the 0.022 wt%, 0.045 wt%, and 0.066 wt% $CaCO_3$ gasifying agent added to the TiC-50 wt% Ni_3Ti are presented in Fig. 13. The photomicrographs show larger TiC particles as the amount of $CaCO_3$ additive is increased. An increase in the amount of intermetallic (Ni_3Ti) is also observed for increasing amounts of gasifying agent. Burning velocity for the TiC-50 wt% Ni_3Ti with $CaCO_3$ increased for increasing amounts of the gasifying additive. This should result in decreased cooling time, less Ostwald ripening and smaller TiC particles. This is clearly not observed in the SEM photomicrographs. The thermal diffusivity of the TiC-50 wt% Ni_3Ti along with

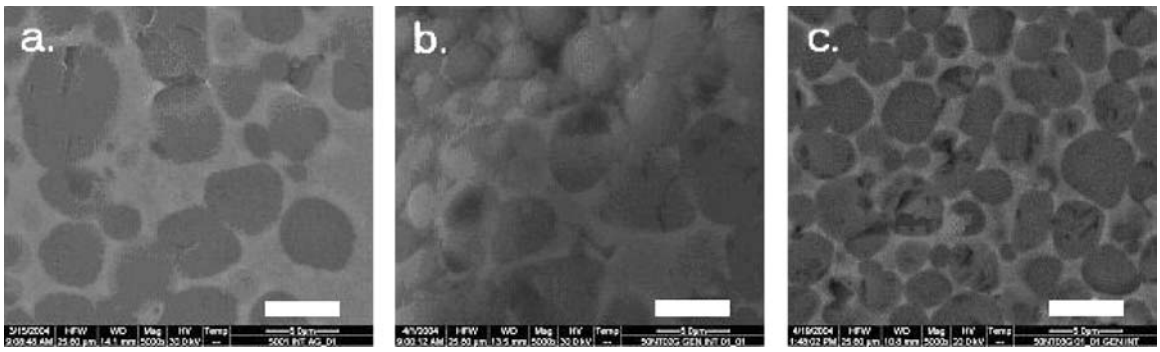

Figure 15 SEM photomicrographs of TiC-50 wt% Ni_3Ti with (a) 0.012 wt%, (b) 0.025 wt% and (c) 0.036 wt% Ca_3N_2 gasifying agent (Scale = 5.0 μm).

the thermal properties of the stable CO_2 play a role in the cooling time of the sample that is effectively increased, as observed from the SEM photomicrographs, for this chemistry and gasifying additive.

XRD profiles for TiC-50 wt% Ni_3Ti with Ca_3N_2 gasifying agent are provided in Fig. 14. The profiles in Fig. 14 are normalized against the 0.012 wt% Ca_3N_2 gasifying agent addition that produces the highest intensity TiC peak. The TiC peak intensity decreased with increasing amounts of Ca_3N_2 gasifying agent. The Ni_3Ti peak intensity does not vary with increasing amounts of Ca_3N_2 gasifying agent. Trace amounts of CaO resulting from the calcium gas oxidizing after the combustion chamber is opened are observed. In addition, trace amounts of nickel and carbon are observed in the XRD patterns as a result of titanium reaction with nitrogen gas.

SEM photomicrographs of the 0.012 wt%, 0.025 wt%, and 0.036 wt% Ca_3N_2 gasifying agent added to the TiC-50 wt% Ni_3Ti chemistry are presented in Fig. 15. The photomicrographs show a decrease in TiC particle size with an increase in the number of TiC particles present as the amount of Ca_3N_2 additive is increased. These photomicrograph observations are in correlation with the increased burning velocity of the reaction that results in decreased cooling time and minimized Ostwald ripening effects.

5. Conclusions

The following conclusions were reached through investigations for the TiC-30 wt% Ni_3Ti and TiC-50 wt% Ni_3Ti with Ca_3N_2 and $CaCO_3$ gasifying agents:

- Addition of Ca_3N_2 and $CaCO_3$ gasifying agents does not affect combustion temperature of the combustion synthesis reaction.
- Ignition characteristics and burning velocities of the combustion reactions are affected by the addition of Ca_3N_2 and $CaCO_3$ gasifying agents.
- The substoichiometric nature of TiC promotes formation of Ni_3Ti intermetallic rather than NiTi. The gasifying additives affect the burning velocities of the reactions and therefore the cooling rate of the samples. The combustion temperature and cooling rate determine the size and number of the TiC particles in the product microstructure. Trace amounts of CaO, nickel and carbon are observed in the product microstructure as a result of TiN and TiO/TiO_2 trigger reactions.

Acknowledgements

The authors wish to thank the Director of the Center for Commercial Applications of Combustion in Space, Dr. Michael Duke, for support of this work. The authors appreciate help from Mrs. Lisa Robinson of Guigne International Limited for assistance with the combustion experiments, Mr. Scott Pawelka with laboratory hardware support and Mr. Gary Zito for assistance with the SEM work of CSM.

References

1 Z. A. MUNIR and U. ANSLEMI-TAMBURINI, *Mater. Sci. Report* **3** (1989) 227.
2 Z. A. MUNIR, *Ceram. Bull.* **67** (1988) 342.
3 J. J. MOORE, F. D. SCHOWENGERDT, R. AYERS, X. ZHANG, and M. CASTILLO, Sixth International Microgravity Combustion Workshop, NASA/CP-2001-210826 (2001) 273.
4 S. F. HULBERT, F. A. YOUNG, R. S. MATHEWS, J. J. KLAWITTER, C. D. TALBERT, and F. H. STELLING, *J. Biomed. Mater. Res.* **4** (1970) 433.
5 S. P. VAN EEDEN, and U. RIPAMONTI, *Plastic and Reconstructive Surgery* **93** (1994) 959.
6 R.W. RICE and W.J. MCDONOUGH, *J. Am. Ceram. Soc.* **68** (1985) C-122.
7 D. E. BURKES, G. GOTTOLI, J. J. MOORE, H. C. YI and R. A. AYERS, *Mat. Res. Soc. Symp. Proc.* **800** (2004) AA4.5.1.
8 R. M. GERMAN, Particle Packing Characteristics, Metal Powder Industries Federation (New Jersey, 1989).
9 R. J. WAKEMAN, *Powder Technology* **11** (1975) 297.
10 D. E. BURKES, J. J. MOORE, G. GOTTOLI, H. C. YI and R. A. AYERS, submitted to *J. Mater. Sci.*, March 2005.
11 V. A. SCHERBAKOV and A. G. MERZHANOV, *Combust. Sci. and Tech.* **136** (1998) 253–277.
12 D. E. BURKES, J. MILWID, G. GOTTOLI and J. J. MOORE, submitted to *J. Mater. Sci.*, 2005.
13 D. E. BURKES, G. GOTTOLI, J. J. MOORE and H. C. YI, accepted by *Met. Mat. Trans. A*, 2005.
14 R. B. KLIMEK, T. W. WRIGHT and R. S. SIELKEN, NASA TM-107144 (1996).
15 J. C. LASALVIA and M. A. MEYERS, *Met. Mat. Trans.* A **26A** (1995) 3011.

16 R. E. REED-HILL and R. ABBASCHIAN, Physical Metallurgy Principles, 3rd ed., (PWS Publishing Company, 1994).
17 A. S. ROGACHEV, A. S. MUKAS'YAN and A. G. MERZHANOV, *Dokl. Akad. Nauk. SSSR (Engl. Trans.)* **297** (1987) 1425–1428.
18 E. A. OLEVSKY, E. R. STRUTT and M. A. MEYERS, *J. Mater. Proc. Tech.* **121** (2002) 157.
19 Y. CHOI, and S.-W. RHEE, *J. Mater. Sci.* **30** (1995) 4637.
20 C. J. QUINN and D. L. KOHLSTEDT, *J. Amer. Ceram. Soc.* **67** (1984) 305.

Received 17 December 2004
and accepted 17 June 2005